Journal of Solid State Chemistry **150,** 266–275 (2000)
doi:10.1006/jssc.1999.8587, available online at http://www.idealibrary.com on IDEAL®

The Crystal Structures of Thallium(I) Fluoride

P. Berastegui* and S. Hull†,[1]

*Department of Inorganic Chemistry, Arrhenius Laboratory, Stockholm University, S-106 91 Stockholm, Sweden; and
†The ISIS Facility, Rutherford Appleton Laboratory, Chilton, Didcot, Oxfordshire, OX11 0QX, United Kingdom

Received September 14, 1999; in revised form November 12, 1999; accepted November 22, 1999

The effects of temperature and pressure on the crystal structures of thallium(I) fluoride have been investigated using powder neutron diffraction, with the aim of resolving the uncertainties present in the literature. Under ambient conditions, TlF adopts an orthorhombic structure in space group *Pbcm* with $Z = 4$ and cell parameters $a = 6.09556(8)$ Å, $b = 5.48860(7)$ Å, and $c = 5.18300(7)$ Å. This structure can be derived from an idealized rocksalt-type arrangement, though with extensive distortions of the anion sublattice due to the presence of the $6s^2$ inert pair of the Tl^+ Above 355 K TlF becomes tetragonal with $Z = 2$, $a = 3.78283(2)$ Å, $c = 6.12312(5)$ Å, and space group *P*4/nmm. The behavior of the compound is also studied under hydrostatic pressure but, contrary to previous reports, no structural transition was observed and TlF remains orthorhombic up to at least 3.5 GPa. The compressibility is greatest along the *a* and *b* axes. The relationship between the ambient- and high-temperature structures of TlF is described and the influence of the inert pair discussed in relation to the massicot structured polymorph of PbO.

Key Words: **thallium(I) fluoride; electron lone pairs; neutron diffraction.**

1. INTRODUCTION

The most common crystal structures adopted by binary *AB* compounds are the fourfold coordinated zincblende ($F\bar{4}3m$, $Z = 4$), the sixfold coordinated rocksalt ($Fm\bar{3}m$, $Z = 4$), and the eightfold coordinated CsCl-type ($Pm\bar{3}m$, $Z = 1$) arrangements. The application of hydrostatic pressure favors structural transitions to more densely packed configurations with higher coordination numbers, though the observed changes are strongly dependent on the nature of the bonding between the constituent *A* and *B* species. Thus, many covalently bonded *AB* compounds (such as the III–V and II–VI semiconductors) transform under pressure from their tetrahedrally coordinated zincblende arrangement to the octahedrally coordinated rocksalt structure and/or a distorted variant in space group *Cmcm* with an irregular fivefold coordination (1). At the other extreme, the ionic Na, K, and Rb halides transform from the rocksalt structure to the CsCl type under pressure (2). The CsCl structure represents the densest packing of spheres of comparable size and, ignoring the possibility of metallization under extreme compression at $p > \sim 100$ GPa (3), no further transitions are expected (or observed) in compounds that adopt this structure, such as CsCl, CsBr, and CsI.

The description given above is, of course, a rather simplistic one and there are many exceptions to this picture. Furthermore, the structural behavior of *AB* compounds whose bonding character differs from those discussed above is often rather complex and its relationship to that of the predominantly ionic and covalent compounds is currently an active area of solid state research. For example, the Cu and Ag monohalides can be considered as "I–VII" compounds which are ionic counterparts to the III–V and II–VI semiconductors. The sequence of structural transitions zincblende → rocksalt → CsCl type is observed on decreasing volume, though it occurs via numerous intermediate phases of lower symmetry that have only recently been characterized (4–6). Another exception is the group of binary compounds whose bonding character is influenced by the presence of lone-pair electrons, such as the Pb^{2+} and Sn^{2+} monochalcogenides and the Tl^+ monohalides. The essentially nonspherical nature of the Pb^{2+}, Sn^{2+}, and Tl^+ cations is manifest in their distorted anion environment, and, in the specific case of the Tl^+ compounds, the possibilities of unusual bonding character in compounds such as TlSe and $TlInSe_2$ (7) has attracted a wider interest in their structural behavior. In this context, and as part of a broader research program to investigate the structural properties of *AB* compounds with "unusual" bonding character under pressure and temperature, we have recently performed a series of powder neutron diffraction studies of thallium(I) fluoride. The results of these experiments are described in this paper. However, the ionic arrangement within TlF has been the subject of many previous publications and we first present a brief summary of the literature. Where necessary, the original assignment of the crystallographic axes (and, hence,

[1]To whom correspondence should be addressed. Fax: int +44 1235 445720. E-mail: s.hull@rl.ac.uk.

0022-4596/00 $35.00

TABLE 1

	TlF-II	
Ketelaar (10)	6.080 Å × 5.495 Å × 5.180 Å	*Fmmm* (No. 69)
Barlow and Meredith (11)	6.092 Å × 5.506 Å × 5.190 Å	$Pbc2_1$ (No. 29)
Alcock and Jenkins (12)	6.0980 Å × 5.4916 Å × 5.1848 Å	*P2cm* (No. 28)
	TlF-I	
Pistorius and Clark (9)	3.771 Å × 6.115 Å at 408 K	*I4/mmm* (No. 139)
Barlow and Meredith (11)	3.783 Å × 6.092 Å at 418 K	—
Caranoni *et al.* (13)	3.804 Å × 6.120 Å at 373 K	*I4/mmm* (No. 139)

space group) has been transformed to correspond to those used in our subsequent analysis, which have in turn been chosen to conform to the standard setting described in the "International Tables for Crystallography" (8).

2. REVIEW OF THE LITERATURE

Following Pistorius and Clark (9), we denote the ambient temperature and pressure phase by TlF-II. The three previously proposed structural models for TlF-II are summarized in Table 1. There is good agreement concerning the orthorhombic unit cell, whose volume implies the inclusion of four TlF formula units. However, there is clear uncertainty over the correct space group and, hence, the exact location of the ions. This is due to the difficulties in growing single crystals of TlF and preferred orientation problems during powder diffraction studies (see Section 4.1).

The earliest structural description of TlF-II by Ketelaar (10) using X-ray diffraction methods represents a unique distortion of the rocksalt structure, in which the Tl^+ and F^- are in 4*a* 0,0,0 and 4*b* $\frac{1}{2}$, 0,0 sites of space group *Fmmm*. These positions are identical to those adopted in a rocksalt arrangement, but the ionic arrangement is distorted due to the three different axial lengths. The irregular anion coordination around the Tl^+ appeared to be an example of a structural distortion induced by the presence of the $6s^2$ inert pair, though Dunitz and Orgel (14) subsequently noted that the Tl^+ environment is centrosymmetric and inert-pair distortions are required to be noncentrosymmetric. Barlow and Meredith (11) observed a number of additional weak reflections that violated the presence of a face-centered lattice, in

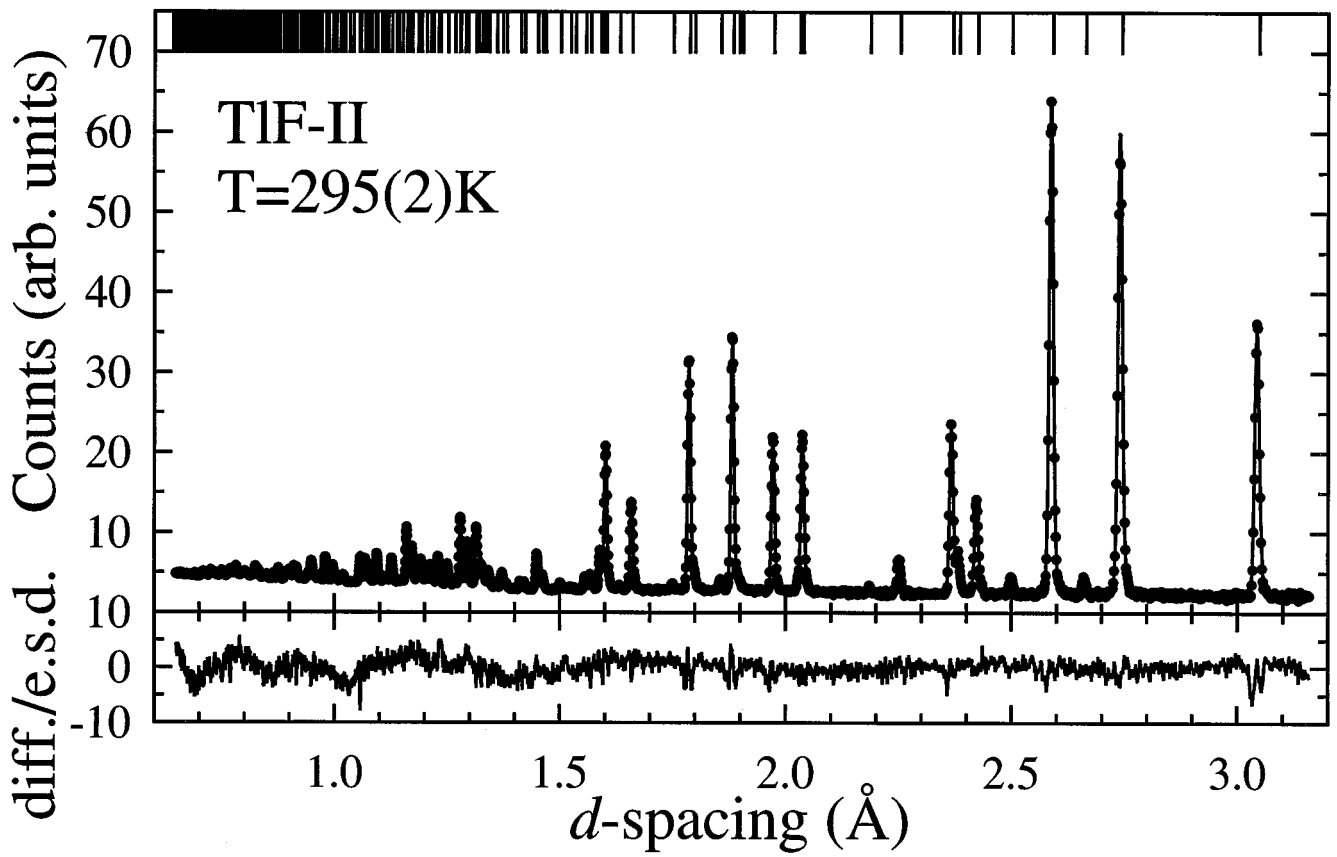

FIG. 1. Rietveld analysis of time-of-flight neutron diffraction data collected from TlF-II at room temperature. The dots are the experimental data points, the line represents the calculated profile, and the tick marks illustrate the calculated peak positions. The lower trace illustrates the difference (measured minus calculated) divided by the estimated standard deviation on the data points.

TABLE 2

	TlF-II	Yellow PbO (27)	TlF-I
Phase temperature	Ambient	Ambient	363(4) K
Space group	*Pbcm*	*Pbcm*	*P4/nmm*
Lattice parameters	$a = 6.09556(8)$ Å	$a = 5.8931(1)$ Å	$a = b = 3.78283(2)$ Å
	$b = 5.48860(7)$ Å	$b = 5.4904(1)$ Å	$c = 6.12312(5)$ Å
	$c = 5.18300(7)$ Å	$c = 4.7528(1)$ Å	
Unit cell volume per formula unit	$V/Z = 43.3507(9)$ Å^3	$V/Z = 38.445(3)$ Å^3	$V/Z = 43.8103(4)$ Å^3
Atomic positions	Tl^+ in 4*d* at $x,y,\frac{1}{4}$	Pb^{2+} in 4*d* at $x,y,\frac{1}{4}$	Tl^+ in 2*c* at $\frac{1}{4}, \frac{1}{4}, z$
	$x_{Tl} = 0.2550(2)$	$x_{Pb} = 0.2297(2)$	$z_{Tl} = 0.2539(2)$
	$Y_{Tl} = 0.0096(2)$	$y_{Pb} = -0.0116(3)$	
	F^- in 4*d* at $x,y,\frac{1}{4}$	O^{2-} in 4*d* at $x,y,\frac{1}{4}$	F^- in 2*c* at $\frac{1}{4}, \frac{1}{4}, z$
	$x_F = -0.1407(2)$	$x_O = -0.1347(3)$	$z_F = -0.1426(2)$
	$y_F = 0.0628(2)$	$y_O = 0.0917(3)$	
Thermal parameters	$B_{Tl} = 1.92(2)$ Å^2	$B_{Pb} = 1.07(3)$ Å^2	$B_{Tl} = 2.42(2)$ Å^2
	$B_F = 2.36(2)$ Å^2	$B_O = 1.14(5)$ Å^2	$B_F = 3.78(3)$ Å^2
Interatomic distances (Å)	Tl^+–F^-	Pb^{2+}–O^{2-}	Tl^+–F^-
	$1 \times 2.430(1)$	$1 \times 2.221(2)$	$1 \times 2.428(1)$
	$1 \times 2.549(1)$	$1 \times 2.249(2)$	$4 \times 2.760(1)$
	$2 \times 2.713(1)$	$2 \times 2.481(1)$	$1 \times 3.695(1)$
	$1 \times 3.116(1)$	$1 \times 3.359(2)$	
	$1 \times 3.695(1)$	$1 \times 3.788(2)$	
	Tl^+–TI^+	PB^{2+}–Pb^{2+}	Tl^+–TI^+
	$2 \times 3.699(1)$	$2 \times 3.536(2)$	$4 \times 3.783(1)$
	$2 \times 3.852(1)$	$2 \times 3.605(1)$	$4 \times 4.029(1)$
	$2 \times 2.956(1)$	$2 \times 3.728(1)$	$4 \times 4.102(1)$
	$2 \times 4.049(1)$	$2 \times 3.856(1)$	
	$2 \times 4.056(1)$	$2 \times 3.977(2)$	
	$2 \times 4.147(1)$	$2 \times 4.205(2)$	
	F^-–F^-	O^{2-}–O^{2-}	F^-–F^-
	$2 \times 3.183(1)$	$2 \times 2.944(2)$	$4 \times 3.195(1)$
	$2 \times 3.236(1)$	$2 \times 3.030(3)$	$4 \times 3.783(1)$
	$2 \times 3.307(1)$	$2 \times 3.171(2)$	
	$2 \times 4.302(1)$	$2 \times 4.441(1)$	
R factors	$R_w = 1.78\%$	$R_w = 8.46\%$	$R_w = 1.55\%$
	$R_{exp} = 1.50\%$	Not given	$R_{exp} = 1.06\%$
Number of data points	$N_d = 2641$	$N_d = 2623$	$N_d = 3169$
Number of peaks	$N_p = 376$	$N_p = 98$	$N_p = 127$
Number of variables	$N_v = 27$	Not given	$N_v = 16$

particular *h*00 reflections with *h* odd and 0*kl* reflections with $k + l$ odd. The full set of observed systematic absences led to the proposal of possible space groups $Pbc2_1$ and *Pbcm*, of which the former was chosen because it can generate a structure approximating that of rocksalt if the Tl^+ and F^- are both placed in general 4*a* *x*,*y*,*z* positions with appropriately chosen values of the fractional coordinates (11). A later diffraction study by Alcock and Jenkins (12) questioned the assignment of space groups $Pbc2_1$ and *Pbcm* on the basis of a very weak 012 reflection that violates the condition 0*kl*, *k* even. The three resultant possible space groups are then *P*2*cm*, $Pmc2_1$, and *Pmcm*, with the former selected as the only assignment that allows an ionic arrangement similar to that of rocksalt. This choice was confirmed by refinements of the data using the other space groups giving higher goodness-of-fit *R* factors (12). However, space group *P*2*cm* requires there to be two symmetry-independent pairs of anions and cations in 2*c* $x,y,\frac{1}{4}$ sites (labeled Tl1, Tl2, F1, and F2), this structure being identical to the $Pbc2_1$ model of Barlow and Meredith (11) if the ionic coordinates satisfy the conditions $y_{Tl1} = -y_{Tl2}$ and $y_{F1} = -y_{F2}$.

On increasing temperature a structural transition has been observed at $\sim$355 K by differential thermal analysis (DTA) (9), drop calorimetry (15), and X-ray diffraction (11) methods. The structure of the high-temperature modification [labeled TlF-I (9)] has been studied by X-ray diffraction and the results are summarized in Table 1. In common with TlF-II, there is a consensus on the unit cell. Pistorius and Clark (9) observed the systematic absences of the reflections to be consistent with a number of body-centered space groups. However, the close relationship between the unit cell constants of TlF-I and those of TlF-II (i.e.,

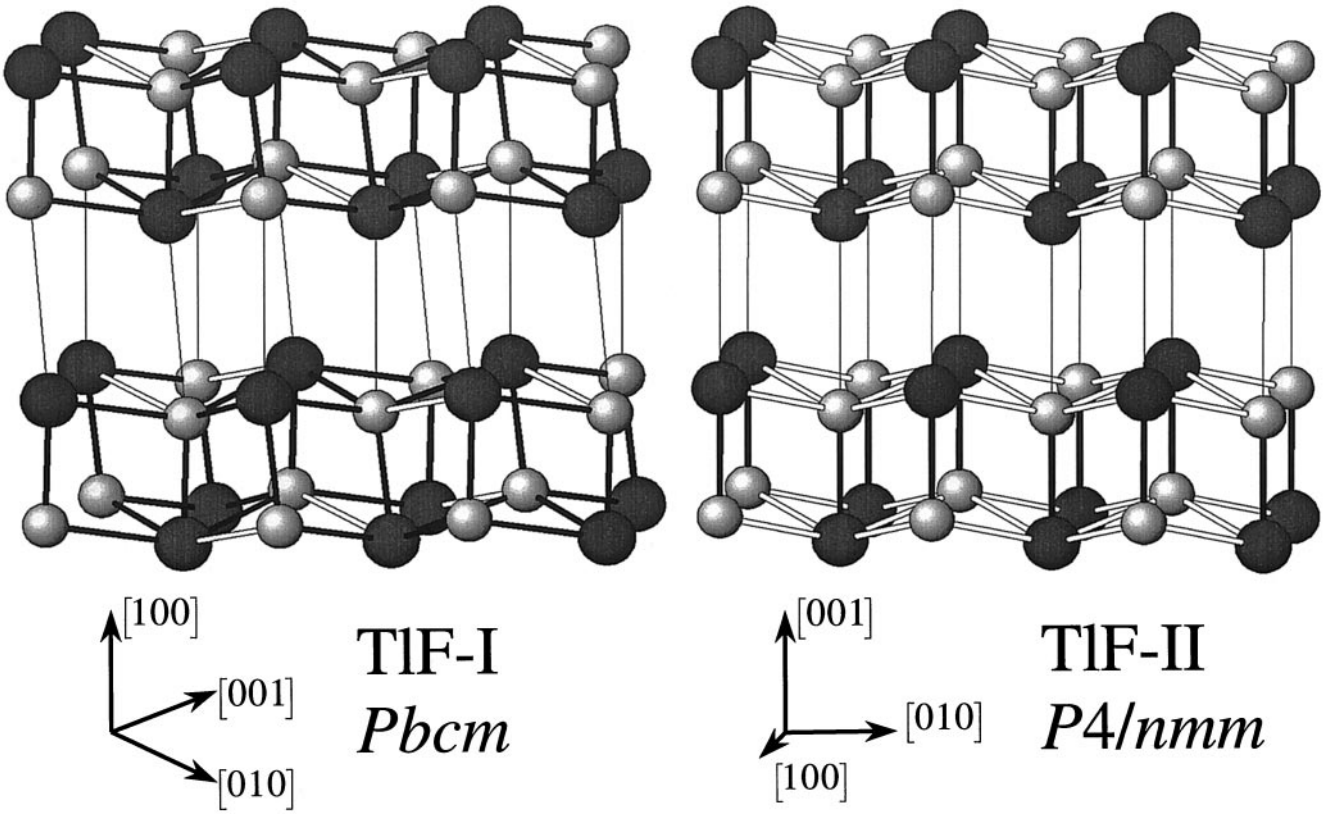

FIG. 2. Crystal structures of TlF-II (left) and TlF-I (right). The larger and smaller spheres represent Tl^+ and F^-, respectively. For TlF-II, the darker bonds denote the Tl^+–F^- distances less than 2.8 Å, and the light bonds denote the slightly longer contact of 3.116(1) Å. In the case of TlF-I, the darker bonds denote the single shorter distance of 2.428(1) Å and the lighter bonds are all equal at 2.760(1) Å. In both cases the narrow lines illustrate the longer Tl^+–F^- distances of $\sim$3.7 Å between the predominantly van der Waals-bonded layers.

$\sqrt{2} \times a_{\text{TlF-I}} \sim b_{\text{TlF-II}} \sim c_{\text{TlF-II}}$ and $c_{\text{TlF-I}} \sim a_{\text{TlF-II}}$), and the general similarity between the observed X-ray diffraction patterns collected from the two phases implied that TlF-I adopted a tetragonally distorted rocksalt arrangement. This can straightforwardly be achieved using space group $I4/mmm$ if the Tl^+ are placed in $2a$ 0,0,0 sites and the F^- are located in the $2b$ 0,0,$\frac{1}{2}$ positions. Calculations of the structure factors using this model were found to agree well with those measured by Caranoni *et al.* (13). In this arrangement the environments around the Tl^+ and F^- are identical and each has four neighboring unlike ions at a distance $a/\sqrt{2}$ in the (001) plane and two further unlike ions at a distance $c/2$ along the [001] axis. However, this structure has been questioned by NMR studies of TlF at elevated temperatures which show differing ^{205}Tl and ^{19}F chemical shifts (16), indicating that the coordination polyhedra around each ion are different.

High-pressure DTA measurements by Pistorius and Clark (9) indicated that TlF-II transforms to a high-pressure modification (TlF-III) at a pressure of 1.3 GPa at ambient temperature, with the TlF-I–TlF-II–TlF-III triple point located at $p = 0.83$ GPa/$T = 332$ K. No diffraction studies of TlF-III have been reported. Assuming a rocksalt-related structure for TlF-II one might expect a transformation to a CsCl-type arrangement under compression. However, the estimated volume change at the transition of only $\sim$0.1% indicates no significant increase in the coordination number and suggests that TlF-III might possess a rocksalt-related structure such as that adopted by the Pb chalcogenides (17) or the alkali metal hydroxides (18). Another possibility is the NiAs-type structure, which is the hexagonal equivalent of the rocksalt arrangement but can be more densely packed if the ratio of the hexagonal unit cell constants c/a exceeds $\sqrt{8/3}$. Indeed, an intermediate phase with the NiAs-type arrangement has recently been observed between the rocksalt and CsCl-type phases in AgF, albeit only on decreasing pressure (6)

3. EXPERIMENTAL

A sample of TlF of purity 99% supplied by Alfa Chemicals Ltd. was used in the experiments after drying at

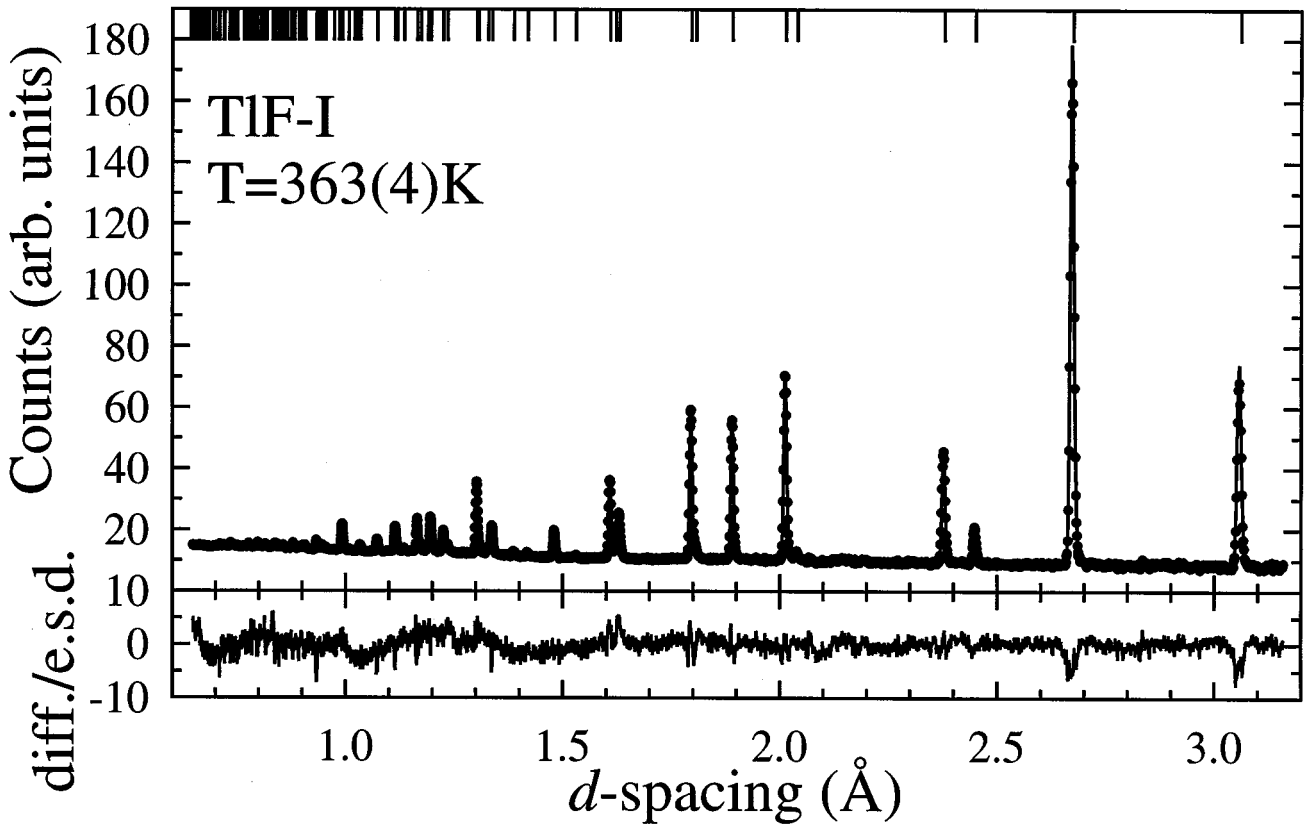

FIG. 3. Rietveld analysis of time-of-flight neutron diffraction data collected from TlF-I at 363(4) K. The dots are the experimental data points, the line represents the calculated profile, and the tick marks illustrate the calculated peak positions. The lower trace illustrates the difference (measured minus calculated) divided by the estimated standard deviation on the data points.

$\sim$395 K but without further purification. Preliminary X-ray diffraction data were collected using a D5000 Siemens powder diffractometer with Cu$K\alpha_1$ radiation and a ground TlF sample on a zero-background sample holder. The majority of the experiments used neutron diffraction and were performed using the Polaris powder diffractometer at the ISIS facility, Rutherford Appleton Laboratory, United Kingdom (19). Measurements at ambient pressure were carried out using an approximately 6-g sample encapsulated inside a thin-walled vanadium can. Diffraction data were collected for about 2 h using the backscattering banks covering the scattering angles $130^\circ < \pm 2\theta < 160^\circ$ and providing data over the d-spacing range $0.2 < d$ (Å) < 3.2 with a resolution $\Delta d/d \sim 5 \times 10^{-3}$. High-pressure experiments were performed using an opposed anvil pressure cell with a sample volume of $\sim 100\,\text{mm}^3$ (20). Pressure calibration was determined using a mixed sample of TlF + NaCl (in the approximate ratio of 4:1 by volume) and the equation of state given by Decker (21). Investigations of the detailed structural pressure dependence used data collected from pure TlF. Approximately hydrostatic conditions were maintained by loading the powder samples with fluorinert as the pressure transmitting medium. For the high-pressure experiments, data were collected using the detector banks that cover the scattering angles $84^\circ < \pm 2\theta < 96^\circ$ and provide data over the d-spacing range $0.3 < d$ (Å) < 4.3 with a resolution $\Delta d/d \sim 6 \times 10^{-3}$. Diffraction data were corrected for the effects of beam attenuation by the cell components and within the sample itself. Details of this procedure can be found elsewhere (22). Typical counting times were 2 h for the pressure calibration and $\sim$10 h to collect diffraction data for structural refinements. Rietveld analyses of the neutron diffraction data used the program TF12LS (23) and coherent scattering lengths of $b_{\text{Tl}} = 8.776$ fm and $b_{\text{F}} = 5.654$ fm (24). The quality of the fits to the experimental data was assessed using the weighted R factor R_{W}, defined in the manner described in the "International Tables for Crystallography" (25). The weighting of the individual points used the squared reciprocal of the estimated standard deviation (e.s.d.) on the data, which are in turn derived from the counting statistics. The relatively low values of R_{W} and the expected R factor R_{exp} are a consequence of the high counting statistics.

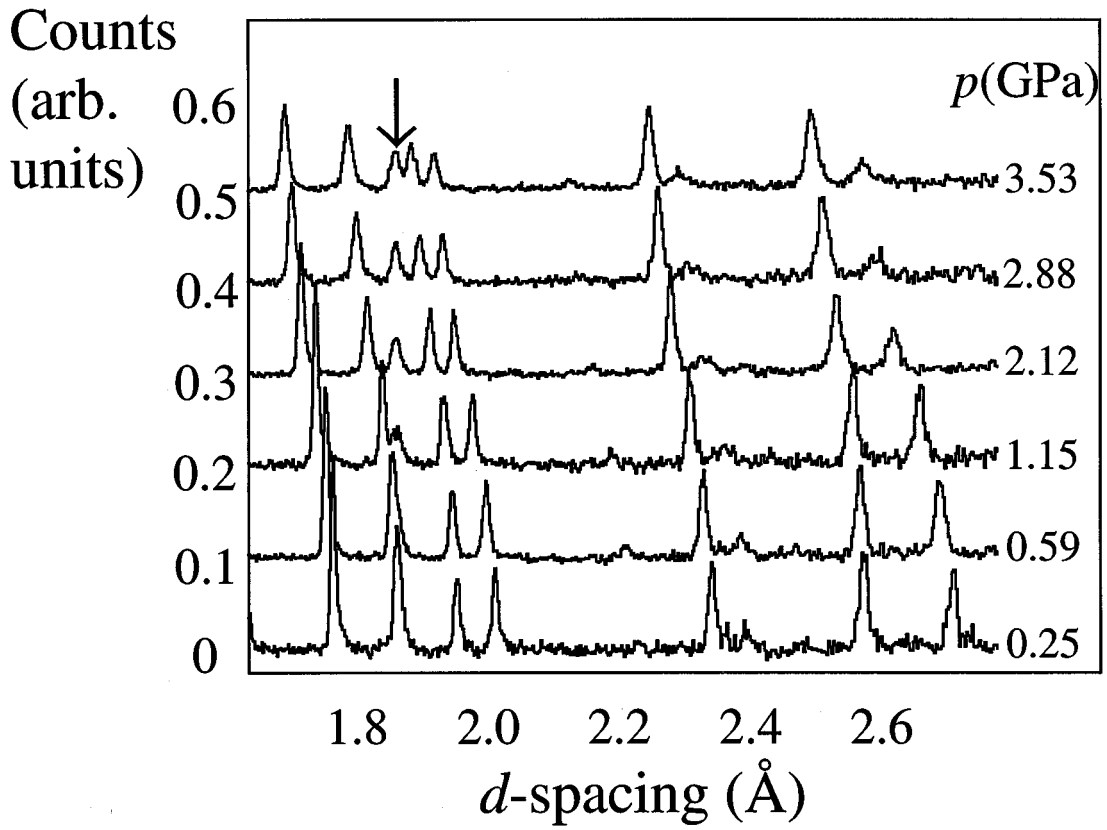

FIG. 4. Evolution of the diffraction pattern of TlF-II with increasing pressure. The peak marked with the arrow originates from tungsten carbide within the anvils of the pressure cell.

4. RESULTS AND DISCUSSION

4.1. Ambient-Temperature TlF-II

The powder diffraction data collected from TlF-II under ambient conditions using both X-ray and neutron radiation could be indexed using an orthorhombic unit cell with approximately $a = 6.096$ Å, $b = 5.489$ Å, and $c = 5.183$ Å. The observed reflection conditions of $0kl$, k even; $h0l$, l even; $0k0$, k even; and $00l$, l even are consistent with space groups $Pbc2_1$ and *Pbcm*. The former corresponds to that proposed by Barlow and Meredith (11) and refinements of the neutron diffraction data were performed using their values of positional coordinates as starting values. The fit to the data converged satisfactorily, though with significant misfit of the intensities. The disagreement between measured and calculated intensities was most noticeable for reflections with a significant h component and could be virtually removed by the inclusion of a preferred orientation correction (26) along the a axis. The tendency for TlF to form thin flakes with their short axis along [100] has been noted previously (12). The final refinement in space group $Pbc2_1$ gave a goodness-of-fit $R_W = 1.91$.

Consideration of the alternative space group, *Pbcm*, shows that a closely related structural arrangement can be obtained if the Tl^+ and F^- are both placed in $4d$ $x,y,\frac{1}{4}$ sites with $x_{Tl} \sim \frac{1}{4}$, $y_{Tl} \sim 0$, $x_F \sim -\frac{1}{4}$, and $y_F \sim 0$. Refinements using space group *Pbcm*, including the preferred orientation correction mentioned above, converged to a significantly lower R factor ($R_W = 1.78$) than the previous space group. The fit to the experimental data is shown in Fig. 1, the resultant structural parameters are listed in Table 2, and the crystal structure is illustrated in Fig. 2.

In asserting that the correct space group for TlF-II is *Pbcm* it is, nevertheless, important to discuss the previous suggestion of Alcock and Jenkins (12). As discussed in Section 2, their assignment of space group *P2cm* was based on the observation using X-ray diffraction of a single weak reflection (012 when referred to our axes) which violates the $0kl$, k even condition imposed by space groups $Pbc2_1$ and *Pbcm*. Simulations of the X-ray diffraction expected from the *P2cm* structural model proposed by Alcock and Jenkins (12) do indeed generate a very weak 012 peak. However, the intensity of this reflection (and other $0kl$ peaks with k odd) is more significant in the case of neutron diffraction and would

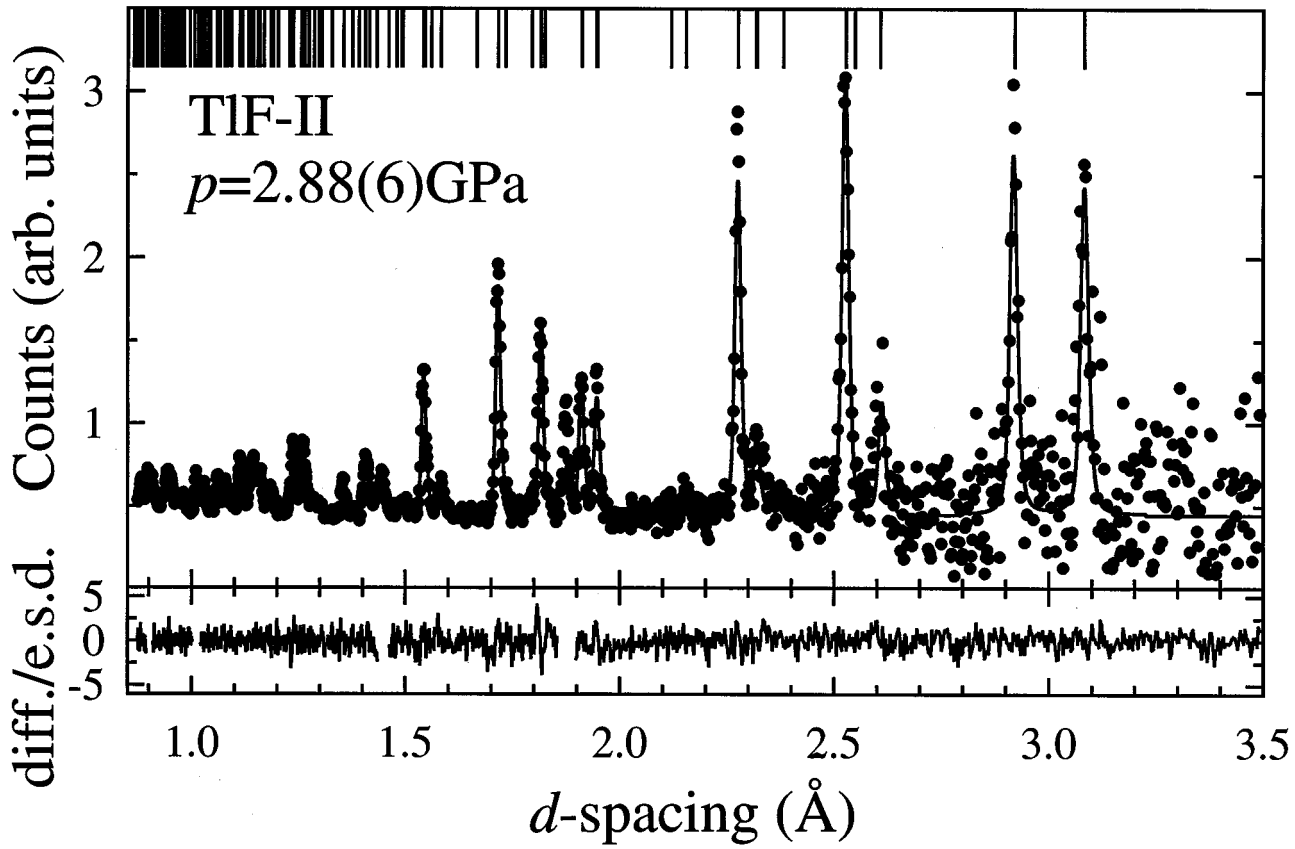

FIG. 5. Rietveld analysis of time-of-flight neutron diffraction data of TlF-II collected at ambient temperature and $p = 2.88(6)$ GPa. The dots are the experimental data points, the line represents the calculated profile, and the tick marks illustrate the calculated peak positions. The lower trace illustrates the difference (measured minus calculated) divided by the estimated standard deviation on the data points. The data points in the vicinity of the tungsten carbide peaks from the pressure cell anvils are excluded from the fit, and the data have been corrected for the effects of attenuation of the beam by the pressure cell components (22).

be observable in our experimental pattern. On these grounds, the *P*2*cm* model appears to be incorrect. This is confirmed by attempts to fit the data using this model, which fail to converge due to excessive correlations between the thermal parameters of the two independent Tl^+ and F^- pairs which are, in the correct *Pbcm* description, related by symmetry.

The crystal structure of TlF-II illustrated in Fig. 2 possesses an almost regular fcc array of Tl^+ which is slightly distorted by the introduction of double layers of F^- between every second layer of Tl^+. This gives rise to sheets of atoms 3.11 Å thick separated by 2.99 Å in the [100] direction. The Tl^+ are on the surface of these layers, which are corrugated parallel to [001]. The sheets are presumably bonded together predominantly by van der Waals interactions between the inert-pair orbitals on the Tl^+. This structure is essentially that of the massicot (β) form of PbO, though in this case the distance between the sheets of Pb^{2+} and O^{2-} (3.19 Å) actually exceeds their thickness (2.71 Å) (27). For comparison, the structural parameters for β-PbO obtained by neutron diffraction (27) are included in Table 2.

4.2. *High-Temperature TlF-I*

The neutron diffraction data collected from TlF-I at 363(4) K could be successfully indexed using a tetragonal unit cell with approximately $a = 3.783$ Å and $c = 6.123$ Å, in accord with previous investigations using X-ray diffraction (see Table 1). However, the neutron diffraction pattern contains numerous reflections that violate the body-centered *hkl*, $h + k + l$ even condition imposed by the previously proposed space group of *I*4/*mmm*, including, for example, the *111* at 2.45 Å and *102* at 2.38 Å. The observed reflection conditions, *hk*0, $h + k$ even and 0*k*0, *k* even are consistent with the two space groups *P*4/*n* and *P*4/*nmm*. However, the volume of the unit cell of TlF-I is approximately half that of TlF-II, which indicates that the unit cell contains two formula units. If we assume that the structure

of TlF-I is ordered then it is necessary to consider only the twofold sites, which are identical in both space groups. By convention, we therefore adopt the higher symmetry case of *P*4/*nmm*.

Recalling that the structure of TlF-II is very similar to that of β-PbO, a first attempt to locate the positions of the ions within TlF-I assumed that it adopts the litharge arrangement of α-PbO, since the latter possesses a similar-sized tetragonal unit cell and the same space group (18). However, simulations of the neutron diffraction pattern with the Tl^+ and F^- placed in "typical" positions for such a litharge-type structure were in poor agreement with that observed. Instead, we recall that the unit cells of TlF-I and TlF-II are closely related ($\sqrt{2} \times a_{\text{TlF-I}} \sim b_{\text{TlF-II}}$ and $c_{\text{TlF-II}}$, $c_{\text{TlF-I}} \sim a_{\text{TlF-II}}$) and that the previously reported X-ray diffraction patterns for TlF-I are close to being body centered. Since X-ray diffraction is dominated by the scattering from the heavier cations, we assume that the Tl^+ in TlF-I are in an approximately fcc arrangement, which requires them to reside in $2c$ $\frac{1}{4},\frac{1}{4},z$ sites with $z_{\text{Tl}} \sim \frac{1}{4}$. On steric grounds, we therefore place the F^- in the $2c$ sites with $z_{\text{F}} \sim -\frac{1}{4}$. Refinements of the data from this starting model converged rapidly, providing a good fit with $R_{\text{W}} = 1.55$ and the parameters listed in Table 2. The quality of the fit to the experimental data is illustrated in Fig. 3.

To the best of our knowledge, the only compound proposed to adopt a tetragonal structure of this type is ZrS (28), though the positions of the two species ($z_{\text{Zr}} = 0.19$ and $z_{\text{S}} = -0.31$) result in a rather different ionic arrangement. However, as illustrated in Fig. 2, there is a close similarity between the structures of TlF-II and TlF-I. In the latter, the thickness of the double sheets and their spacing are equal along the *c* axis at $\sim$3.00 Å. The expansion of the structure with temperature is larger perpendicular to the layers, because the Tl^+–F^- bond lengths along the *c* axis remain essentially equal but the Tl^+–F^-–Tl^+ angle straightens from 168.7° to 180°. TlF-I can thus be considered to be a higher-symmetry counterpart to TlF-II. To further illustrate their interrelationship it is instructive to note that both can be derived from the rocksalt structure. In the case of TlF-II, this occurs if $a_{\text{TlF-II}} = b_{\text{TlF-II}} = c_{\text{TlF-II}}$ and the positional parameters have values $x_{\text{Tl}} = \frac{1}{4}$, $y_{\text{Tl}} = 0$, $x_{\text{F}} = -\frac{1}{4}$ and $y_{\text{F}} = 0$. For TlF-I the requirements are $\sqrt{2}a_{\text{TlF-I}}$ $(= \sqrt{2}b_{\text{TlF-I}}) = c_{\text{TlF-I}}$ with $z_{\text{Tl}} = \frac{1}{4}$ and $z_{\text{F}} = -\frac{1}{4}$. With reference to Table 2, it is clear that in both phases the anion positions are significantly displaced from the rocksalt positions, while the Tl^+ are close to their "ideal" locations and form an approximately fcc sublattice.

4.3. High Pressure

As illustrated in Fig. 4, the diffraction pattern on increasing pressure shows no evidence of a structural phase transition from TlF-II to the phase TlF-III at $p \sim 1.3$ GPa as reported previously (9). At all pressures up to the maximum reached in this work ($p = 3.53$ GPa) the diffraction data could be successfully fitted using the structural model for TlF-II discussed in Section 4.1. This is illustrated in Fig. 5 for the case of the data collected at $p = 2.88(6)$ GPa.

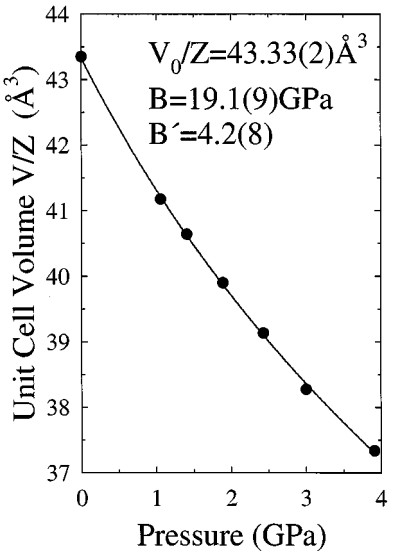

FIG. 6. Compressibility of TlF-II. The full curve represents a fit to the data using a Birch equation (29) to determine the bulk modulus.

The compressibility of TlF-II obtained from these refinements is shown in Fig. 6. The Bulk modulus, obtained by fitting a Birch equation (29) to these data, yields a value of $B = 19.1(9)$ GPa, with a pressure derivative $B' = 4.2(8)$ and a fitted value of the unit cell volume per formula unit at zero

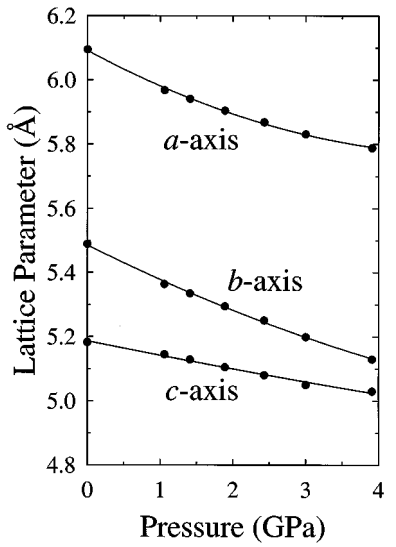

FIG. 7. Evolution of lattice parameters with pressure for TlF-II, illustrating its anisotropic compressibility.

TABLE 3

p (GPa)	a (Å)	b (Å)	c (Å)	V/Z (Å^3)	x_{Tl}	y_{Tl}	x_F	y_F	B_{Tl}	B_F
0.25	6.0592(4)	5.4531(6)	5.1778(6)	42.770(7)	0.246(2)	0.011(1)	− 0.141(1)	0.059(2)	1.9(1)	2.2(2)
0.59	6.0216(2)	5.4113(3)	5.1669(3)	42.090(4)	0.242(1)	0.009(1)	− 0.144(1)	0.056(1)	2.0(1)	2.0(1)
1.15	5.9677(3)	5.3504(5)	5.1443(4)	41.064(5)	0.238(1)	0.009(1)	− 0.143(1)	0.055(1)	1.8(1)	1.9(1)
2.12	5.8904(3)	5.2691(3)	5.0942(3)	39.527(4)	0.232(1)	0.009(1)	− 0.144(1)	0.055(1)	1.8(1)	2.0(2)
2.88	5.8422(5)	5.2159(6)	5.0547(5)	38.507(7)	0.229(2)	0.010(2)	− 0.142(2)	0.050(1)	1.6(2)	2.0(2)
3.53	5.8074(4)	5.1738(4)	5.0228(4)	37.729(5)	0.227(2)	0.010(2)	− 0.142(2)	0.045(2)	1.7(1)	1.8(2)

pressure $V_0/Z = 43.33(2)$ Å^3. The high compressibility of TlF-II is clearly related to its rather open structure. The layered nature of the structure (Fig. 2) might intuitively suggest that the a axis would be the more compressible, though this is not observed in the variation of the individual unit cell lengths with pressure (Fig. 7). Instead, the b axis is the more compressible. A similar observation has been made for the massicot structured phase β-PbO (30). The refined values of the four positional parameters at each pressure are listed in Table 3. Only x_{Tl} and y_F show any significant changes with pressure. The overall effect of the changes in these positional parameters and the anisotropic compression of the unit cell lengths is illustrated in Fig. 8. The Tl^+–F^- distance across the layers remains constant while the shorter distances decrease. As in the case of the high-temperature phase TlF-I (Section 4.2) the Tl^+–F^-–Tl^+ angle along the a axis increases slightly to 172.3° but the major changes are observed within the bc plane. The shortest Tl^+–F^- bond length within the layers and directed along [100] decreases significantly, illustrating that the stereochemistry of the Tl^+ ion induces the inert pair to become highly deformed at high pressures until, presumably, packing considerations favor a structural transition to a CsCl-type arrangement and TlF becomes isostructural with the ambient-pressure forms of TlCl and TlBr (18).

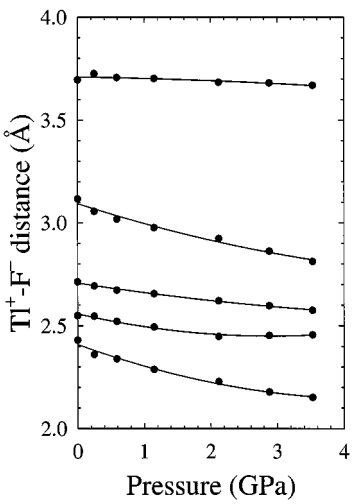

FIG. 8. Variation of Tl^+–F^- bond lengths with pressure in TlF-II.

5. CONCLUSIONS

The structural behavior of thallium(I) fluoride, TlF, which has been the topic of some debate within the literature, has been resolved in this work. The use of neutron diffraction is clearly essential for the study of TlF, since the scattering powers of the constituent ionic species are more comparable for neutrons ($b_F/b_{Tl} = 0.64$) than X rays ($Z_F/Z_{Tl} = 0.11$). This advantage is compounded in the specific case of TlF because the extensive distortion away from the rocksalt arrangement due to the presence of the inert pair affects predominantly the anion sublattice.

The close structural relationship between TlF-II and massicot structured β-PbO is, with hindsight, not surprising, since both contain $6s^2$ inert pairs. However, both were previously believed to be different (and, indeed, unique) structures. Clearly, it is impossible to make generalizations concerning the nature of the inert-pair distortions within binary AB systems on the basis of two compounds, since the heavier halogens and chalcogens do not activate the inert pairs and compounds such as TlCl, TlBr, PbS, PbSe, and PbTe adopt undistorted cubic structures. SnO is a strong candidate to exhibit a massicot structured phase and might [by analogy with PbO (30)] be expected to transform from its ambient litharge structure to massicot under pressure. However, no such transition has been observed up to 7.5 GPa (30). Nevertheless, the similarity between the structures of β-PbO and TlF-II does not support the presence of a "novel" form of Tl^+–Tl^+ interaction proposed recently (7). Similarly, recent interpretations of the different structural behavior of PbO and TlF in terms of detailed differences in their inert-pair interactions (16) are based on incorrect crystallographic data and therefore need to be reassessed.

ACKNOWLEDGMENT

One of us (P.B.) thanks the Swedish Federation for International Cooperation in Research and Higher Education for financial support.

REFERENCES

1. R. J. Nelmes and M. I. McMahon, *Semiconductors Semimet*. **54,** 145 (1998).
2. Y. E. Tonkov, "High Pressure Phase Transformations. A Handbook." Gordon & Breach, London, 1992.
3. M. I. Eremets, K. Shimizu, T. C. Kobayashi, and K. Amaya, *Science* **281,** 1333 (1998).
4. S. Hull and D. A. Keen, *Phys. Rev. B* **50,** 5868 (1994).
5. M. Hofmann, S. Hull, and D. A. Keen, *Phys. Rev. B* **51,** 12022 (1995).
6. S. Hull and P. Berastegui, *J. Phys. Condens. Matter* **10,** 7945 (1998).
7. S. P. Gabuda, S. G. Kozlova, and R. L. Davidovich, *Chem. Phys. Lett*. **263,** 253 (1996).
8. T. Hahn (Ed.), "International Tables for Crystallography." Vol. A. Kluwer, Dordrecht, 1996.
9. C. W. F. T. Pistorius and J. B. Clark, *Phys. Rev*. **173,** 692 (1968).
10. J. A. A. Ketelaar, *Z. Kristallogr*. **92,** 30 (1935).
11. M. Barlow and C. Meredith, *Z. Kristallogr*. **130,** 304 (1969).
12. N. W. Alcock and H. D. B. Jenkins, *J. Chem. Soc. Dalton* **17,** 1907 (1974).
13. C. Caranoni, R. Favier, L. Capella, and A. Tranquard, *C.R. Acad. Sci. Paris*, *Ser. C* **270,** 1795 (1970).
14. J. D. Dunitz and L. E. Orgel, *Adv. Inorg. Chem. Radiochem.* **2,** 42 (1960).
15. D. Cubicciotti and H. Eding, *J. Chem. Eng. Data* **10,** 343 (1965).
16. S. P. Gabuda and S. G. Kozlova, *J. Struct. Chem.* **38,** 140 (1997).
17. T. Chattopadhyay, A. Werner, H. G. von Schnering, and J. Pannetier, *Rev. Phys. Appl*. **19,** 807 (1984).
18. R. W. G. Wyckoff, "Crystal Structures," Vol. 1. Interscience, New York, 1963.
19. S. Hull, R. I. Smith, W. I. F. David, A. C. Hannon, J. Mayers, and R. Cywinsky, *Physica C* **180/181,** 1000 (1992).
20. J. M. Besson, R. J. Nelmes, G. Hamel, J. S. Loveday, G. Weill, and S. Hull, *Physica B* **180/181,** 907 (1992).
21. D. L. Decker, *J. Appl. Phys.* **42,** 3239 (1979).
22. J. S. Loveday, R. J. Nelmes, W. G. Marshall, R. M. Wilson, J. M. Besson, S. Klotz, G. Hamel, and S. Hull, *High Pressure Res.* **14,** 7 (1995).
23. W. I. F. David, R. M. Ibberson, and J. C. Matthewman, Rutherford Appleton Laboratory Report RAL-92-031 (1992).
24. V. F. Sears, *Neutron News* **3,** 26 (1992).
25. A. J. C. Wilson (Ed.), "International Tables for Crystallography," Vol. C. Kluwer, Dordrecht, 1995.
26. A. March, *Z. Kristallogr*. **81,** 285 (1932).
27. R. J. Hill, *Acta Crystallogr. Sect. C* **41,** 1281 (1985).
28. G. Hägg and N. Schönberg, *Ark. Kemi* **40,** 371 (1954).
29. F. Birch, *J. Geophys. Res.* **83,** 1257 (1978).
30. D. M. Adams, A. G. Christy, J. Haines, and S. M. Clark, *Phys. Rev. B* **46,** 11358 (1992).